Jecmenica, M, Brkovic, B, Levi, E and Lazarevic, Z

Interplane cross-saturation in multiphase machines

IET Research Journals

Submission Template for IET Research Journal Papers

Journals
The Institution of Engineering and Technology

Interplane cross-saturation in multiphase machines

ISSN 1751-8644
doi: 0000000000
www.ietdl.org

Milos Jecmenica[1*], Bogdan Brkovic[1], Emil Levi[2], Zoran Lazarevic[1]

[1] Faculty of Electrical Engineering, University of Belgrade, Bulevar Kralja Aleksandra 73, 11000 Belgrade, Serbia
[2] Department of Electronics and Electrical Engineering, Liverpool John Moores University, Byrom Street, Liverpool L3 3AF, UK
* E-mail: jecmenica@etf.bg.ac.rs

Abstract: The use of electrical machines in electric vehicles and high-power drives frequently requires multiphase machines and multiphase inverters. While appropriate mathematical models under the linear magnetic conditions are readily available for multiphase machines, the same cannot be said for the models of the saturated multiphase machines. This paper examines the saturation in an asymmetrical six-phase induction machine under different supply conditions and addresses the applicability of the existing saturated three-phase machine models for representation of saturated multiphase machines. Specifically, the mutual coupling between different sequence planes in the vector space decomposed model under saturated conditions is analyzed. The paper relies on analytical considerations, finite element analysis and experimental results. It is shown that the saturation of the main flux path is influenced by the current components in the orthogonal (non-fundamental) sequence plane. This implies the need to develop new multiphase machine models which take this effect into account.

1 Introduction

During the last fifteen years or so a rapid pace of development has taken place in the area of multiphase (more than three phases) machines and drives. Such machines are suitable for numerous niche applications, due to the advantages offered by the existence of more than three phases (e.g. locomotive traction, electric ship propulsion, very high power industrial applications, electric and hybrid electric vehicles, more-electric aircraft concept, remote off-shore wind energy generation) [1–3].

The control strategies for multiphase drive applications require a good knowledge of the machine parameters to ensure a high quality of the dynamic and steady-state drive performance [4]. The performances of a machine controller, which depend on knowledge of the machine's magnetic properties, can be worsened by the phenomenon of magnetic saturation. Proper understanding and modeling of the saturation phenomenon plays a key role in determining the flux-weakening capability and better control performance of multiphase drives, since the precise estimation of controlled quantities (e.g. machine currents) and the control algorithms are all based on multiphase machine modeling. If such control systems can operate properly in the presence of magnetic saturation, a smaller machine may be used for the same purpose [5].

One of the standard assumptions of the general theory of electrical machines is that the main flux saturation can be neglected. This however proves to be inadequate in many operating regimes of three-phase machines and it is even not possible to study by simulation certain transients under this assumption (e.g. self-excitation of a three-phase stand-alone induction generator). It is for this reason that, over the years, a large research effort has been put into development of modified three-phase machine models that can account for the main flux saturation phenomenon in an accurate way. Nowadays, numerous improved models are available for both three-phase induction and synchronous machines that enable appropriate representation of the saturation within the circuit equations used to describe the machine. In general, three common approaches related to the main flux saturation modeling in three-phase machines can be identified: modeling in phase coordinates [6], d-q model approach [7–12] and voltage-behind-reactance (VBR) approach [13–15]. In many ways, this research topic is now closed as far as the three-phase machinery is concerned.

Since multiphase machines are still not as common in industry as their three-phase counterparts, a huge effort has been made recently to improve multiphase machine parameter estimation techniques [16, 17]. While appropriate mathematical models under the linear magnetic conditions are readily available for multiphase machines [18, 19], the same cannot be said for the models of the saturated multiphase machines. A relatively few works have dealt with this topic [20–23] and there appears to be still a large scope for improvement.

By vector space decomposition (VSD) approach, the original phase-domain model of a multiphase machine can be decomposed into several equivalent circuits that represent the decoupled vector subspaces (planes): the fundamental (dq) plane, identical to that of a three-phase machine, one or multiple orthogonal (xy) planes and one or two zero-sequence components [2]. The advantages of the VSD model regarding the component decoupling become questionable if saturation and mutual leakage between stator windings is considered. The analysis of mutual coupling between the dq and xy planes carried out in [21, 23] assumes a synchronously rotating xy magnetomotive force (mmf) which contributes to air-gap flux and thus to the saturation of the main flux path. On the other hand, xy current components at fundamental frequency generate a subsynchronously rotating mmf which results in a flux density confined to leakage flux paths, due to the rotor cage reaction. Fundamental frequency currents in the xy plane are certain to occur in all post-fault scenarios that exploit fault tolerance [24], in all schemes that suggest power sharing control of the machine with multiple three-phase windings [25–28], as well as in the regenerative testing methods recently developed for multiphase machines [29, 30]. It is unknown if coupling between different orthogonal planes occurs under saturated conditions in such cases. Therefore, it is debatable whether the existing saturated dq machine models can be used to adequately take the magnetic saturation in multiphase machines into account when fundamental-frequency xy current components are present.

For the machine control purposes, it is common to take only the saturation of the main flux path into account. The leakage inductances are not affected by magnetic saturation, which is reasonable except in fault and overload conditions [9]. At low flux values, the inductances remain constant, but as the flux increases the machine starts to saturate and the inductances decrease. This is important when the machine is designed to be slightly saturated in the rated operating point in order to maximize the torque production [31, 32].

In this paper, the influence of fundamental frequency xy plane quantities on the saturation of the main flux path in an asymmetrical six-phase induction machine (6PHIM), with a 30° electrical shift between the two three-phase windings, will be investigated. It will be examined whether the saturation of the main flux path has an effect on the decomposition between the dq and xy planes. The influence of the xy plane on saturation will be investigated analytically, through Finite Element Analysis (FEA), and experimentally. According to the research presented in the following sections, it is concluded that the main flux path occurs mostly due to the torque-producing (dq) plane, but an influence of the orthogonal (xy) plane exists. This mutual influence between subspaces is termed "inter-plane cross-saturation". According to the results obtained from the upcoming analyses, it is not possible to adequately include the saturation effect by considering only the currents in the dq plane, since the effect of the xy plane needs to be included as well.

This paper is organized as follows. The existing linear VSD model and a proposed approach for inclusion of magnetic saturation are described in the second section. An intuitive qualitative approach to the analysis of interplane cross-saturation will be presented in the third section. Results obtained using FEA will be given in the fourth section, whereas the experimental verification is given in the fifth section. The discussion of the results is given in the sixth section, and the conclusions are presented in the final section.

2 Theoretical background

In electrical machine theory, the following assumptions are frequently made when considering saturation phenomena [33]:

- the total flux linkages of each coil are the sum of the leakage and mutual flux components,
- the magnetic circuit saturation depends on the total air gap flux linkages,
- the leakage flux paths are not subject to saturation (except in transients and overload conditions), and
- hysteresis and eddy current effects (iron losses) are neglected.

Three main approaches to multiphase machine modeling exist: phase-variable, multiple dq (for multiphase machines with multiple three-phase windings) and VSD model. The phase-domain has the advantage of directly representing physical quantities, which simplifies the interfacing of the machine model with the power system network and allows more accurate representation of internal machine phenomena. The negative aspect of the phase-variable model is that it consists of nonlinear differential equations with time-varying coefficients, due to variable stator-to-rotor mutual inductances, which is not always easy to solve. The multiple dq model is based on transforming the electrical quantities of each three-phase winding into a rotating reference frame and then merging them into a unified model [18, 19]. This model allows the real behavior of the machine under asymmetrical conditions to be simulated, but is more complicated compared to the VSD model [34]. Despite its many advantages, it is difficult to interface this model with the external components or power electronics circuits modeled in the phase domain. Therefore, the voltage-behind-reactance approach was recently proposed as an alternative solution [21, 22]. The widely used VSD model is based on transforming the phase-domain variables of a multiphase machine into a fundamental (torque-producing) plane, one or more orthogonal (non-torque-producing) planes and one or two zero-sequence subspaces. The fundamental and non-fundamental subspaces are completely decoupled, which provides valuable benefits in terms of machine analysis and control [35, 36]. The VSD model equivalent circuit of a multiphase machine is identical to that of a three-phase machine, making the existing control techniques directly applicable to multiphase machines [34]. This approach can adequately describe the machine in both transient and steady-state operating conditions, both for sinusoidal and non-sinusoidal supply.

Decoupling between subspaces facilitates modeling and control of the machine. The decoupling assumption regarding the VSD model is questionable under saturated conditions. Only the coupling between the dq and xy components will be studied, as the zero-sequence components can always be avoided by simply isolating the neutral points. The 6PHIM is commonly operated with separated neutral points, as this reduces the system dimensionality and thus simplifies the control algorithm [34]. The unsaturated VSD model of a 6PHIM will be presented, followed by an assumed extension to a model involving saturation.

2.1 Unsaturated VSD model

The voltage equations of a 6PHIM in the VSD domain are given as [37]:

$$\begin{aligned} \boldsymbol{u_s} &= \boldsymbol{R_s i_s} + \frac{d\boldsymbol{\psi_s}}{dt} - \omega_e \begin{bmatrix}\psi_{qs} & -\psi_{ds} & 0 & 0 & 0 & 0\end{bmatrix}^T \\ \boldsymbol{0}_{6\times1} &= \boldsymbol{R_r i_r} + \frac{d\boldsymbol{\psi_r}}{dt} - (\omega_e - \omega) \begin{bmatrix}\psi_{qr} & -\psi_{dr} & 0 & 0 & 0 & 0\end{bmatrix}^T \end{aligned} \tag{1}$$

where ω (rad/s) is the rotor electrical angular speed, ω_e (rad/s) is the arbitrary angular speed of the rotating reference frame, and:

$$\begin{aligned} \boldsymbol{\xi_{s,r}} &= \begin{bmatrix}\xi_{ds,r} & \xi_{qs,r} & \xi_{xs,r} & \xi_{ys,r} & \xi_{0+s,r} & \xi_{0-s,r}\end{bmatrix}^T \\ \boldsymbol{R_s} &= R_s \cdot \boldsymbol{I}_{6\times6}, \quad \boldsymbol{R_r} = R_r \cdot \boldsymbol{I}_{6\times6} \end{aligned} \tag{2}$$

where $\boldsymbol{I}_{6\times6}$ is an identity matrix of the sixth order and ξ stands for an arbitrary electrical quantity (voltage, current or flux linkage). The stator flux linkages are given in space vector form as (analogous expressions hold for rotor flux linkages):

$$\vec{\psi}_{dqs} = (L_m + L_{ls})\vec{i}_{dqs} + L_m\vec{i}_{dqr} \tag{3a}$$
$$\vec{\psi}_{xys} = L_{ls}\vec{i}_{xys} \tag{3b}$$
$$\psi_{0+s} = L_{ls} i_{0+s} \tag{3c}$$
$$\psi_{0-s} = L_{ls} i_{0-s}, \tag{3d}$$

where L_m is the magnetizing inductance and L_{ls} is the stator leakage inductance. Note that there is no mutual influence between the quantities of different subspaces. With no saturation involved, all inductances in (3) are constant. The remaining equations needed to complete the model are the torque equation:

$$T_e = pL_m\left(i_{dr}i_{qr} - i_{ds}i_{qs}\right) \tag{4}$$

and the electromechanical motion equation:

$$T_e - T_L = J\frac{d\Omega}{dt} + k_f\Omega, \tag{5}$$

where p is the pole pair number, T_L is the load torque, J is the moment of inertia, $\Omega = \omega/p$ is the mechanical angular rotor speed, and k_f is the friction coefficient. The given equations are obtained when applying the power invariant decoupling transformation matrix [37]. Note that the given model is simplified as mutual leakage inductance is neglected in flux equations (3). According to [38], mutual leakage terms occur in dq and zero-sequence flux equations. This effect is not essential for the analysis in this paper, so it will be discarded for the sake of simplicity.

2.2 Hypothesis - saturation modeling

It is already known from [11, 39] that coupling between windings in spatial quadrature (cross-saturation) exists in saturated smooth air-gap machines. By analogy with this phenomenon, it is of interest to determine if the main flux saturation affects the mutual coupling between the dq and xy planes, that are decoupled under unsaturated conditions. This research is necessary in order to investigate if the cross-coupling effect exists between different VSD subspaces. If it is proven that the multiphase machine main flux saturation can be modeled solely in the fundamental (dq) plane, all existing conclusions regarding the modeling of saturated three-phase machines would apply to multiphase machines as well. It will therefore be assumed that saturation occurs solely under the influence of fundamental (dq) plane components and that non-torque producing subspaces do not contribute to saturation. In other words, it will be considered that the decoupling between the orthogonal subspaces is still valid in saturated conditions. According to this assumption, saturation inclusion in the model requires addition of the following equation to the unsaturated VSD model (1)–(5):

$$L_m = f(i_m), \quad i_m = \sqrt{(i_{ds} + i_{dr})^2 + (i_{qs} + i_{qr})^2}, \qquad (6)$$

where i_m is the magnetizing current of the machine. Note that the decoupling of subsystems is not affected by this modification, as already stated. It is the goal of this paper to confirm or rebut this assumption.

It should be noted that the machine model (1)-(6) is given here in a generic form. Its subsequent formulation in terms of state-space variables would lead to the introduction of the dynamic cross-saturation in the dq equations in accordance with the selected state-space variable set, in the same manner as for a three-phase machine [7–11]. Importantly however, if (6) is sufficient to model the saturation effect then all the three-phase machine dq models become directly applicable to multiphase machines, as xy equations of the model (1)-(3) remain fully decoupled from the dq equations.

3 Analytical approach

It is of interest to determine whether the xy currents affect the reluctance of iron parts of the main flux path and, if so, under which conditions. For this purpose, an appropriate magnetic equivalent circuit of the machine is developed and examined. By solving the circuit equations under different conditions, the influence of xy current components on the saturation of the main flux path can be studied.

3.1 Magnetic equivalent circuit

Only the stator magnetic circuit will be modeled. A part of the circuit spanning an arbitrary slot is shown in Fig. 1. All dimensions displayed in Fig. 1 are defined in Table 3 in the Appendix. The entire model spans one pole pair, i.e. Q_{pp} slots. A similar concept is proposed in [40] for calculating the core reluctance of an induction machine. Given the qualitative nature of the analysis, the following simplifying assumptions are made in this model:

(i) The fundamental air-gap flux (main flux) is sinusoidally distributed and independent of the potential stator winding currents in the xy subspace. The fundamental flux is generated by the dq voltage supply, and will therefore be referred to as the dq flux component (note however that the dq currents are zero);

(ii) Leakage flux caused by the dq current components will be neglected, i.e. it will be considered that only the xy current components contribute to the leakage flux. This assumption goes in hand with (i), as the main flux can now be considered proportional to the supply voltage (provided that the winding resistance is also neglected);

(iii) It will be assumed that reluctances of stator slot bridges are constant, i.e. the slot saturation in the tangential direction will be neglected, as this flux path is dominated by air. Additionally, the flux density over the length of each stator tooth will be considered constant;

(iv) Uniform flux density distribution will be assumed in each part of the magnetic circuit;

(v) A constant flux density will be assumed in each part of the stator yoke between the centerlines of two adjacent teeth (yoke section of length l_{ys} in Fig. 1).

Since the fundamental flux density is predefined, only the non-fundamental flux components generated by the currents in the xy subspace, if present, are left to be determined. Therefore, an mmf corresponding to xy current components is attributed to each slot. The particular mmf values for each slot depend on the layout of the particular winding. According to Fig. 1, the mmf balance equation for an arbitrary slot is then given as:

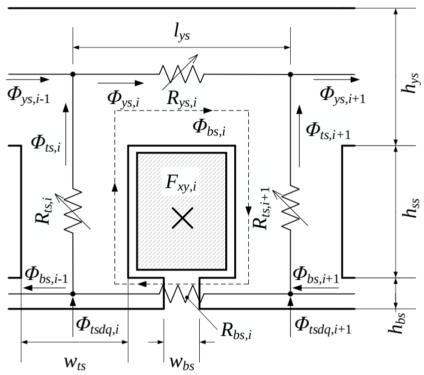

Fig. 1: Part of the developed stator magnetic circuit surrounding one slot

$$F_{xy,i} = \left(R_{bs} + R_{ts,i} + R_{ys,i} + R_{ts,i+1}\right)\Phi_{bs,i}, \qquad (7)$$

where $i \in \{1, \ldots, Q_{pp}\}$, and $\Phi_{bs,i}$ is the self flux corresponding to the i^{th} slot, i.e. the flux generated solely by the slot mmf $F_{xy,i}$. This flux component is designated by a dashed line in Fig. 1. Note that $\Phi_{bs,i}$ is confined to the leakage flux path, which is in accordance with the fact that the xy currents produce only leakage flux [17]. As stated in assumption (iii), the stator slot bridge reluctance R_{bs} is considered constant and equal for each slot. Stator yoke and tooth reluctances depend on the corresponding total flux densities, which are defined as:

$$B_{ys,i} = \frac{\Phi_{bs,i} + \Phi_{ysdq,i}}{h_{ys} l_a}, \qquad (8a)$$

$$B_{ts,i} = \frac{\Phi_{bs,i} + \Phi_{tsdq,i} - \Phi_{bs,i-1}}{w_{ts} l_a}, \qquad (8b)$$

where l_a is the axial length of the machine (Table 3 in the Appendix), $\Phi_{tsdq,i}$ is the main flux through one slot pitch, and $\Phi_{ysdq,i}$ is the yoke flux obtained by integrating the main flux density over the perimeter of the machine. In this model, the yoke flux corresponding to the portion of the yoke above the i^{th} slot is calculated approximately as:

$$\Phi_{ysdq,i} = \sum_{n=1}^{n=i} \Phi_{tsdq,n} \qquad (9)$$

The yoke, tooth, and slot bridge reluctances are given as:

$$R_{ys,i} = \frac{l_{ys}}{\mu_{ys,i}(B_{ys,i}) h_{ys} l_a} \qquad (10a)$$

$$R_{ts,i} = \frac{h_{ss}}{\mu_{ts,i}(B_{ts,i}) w_{ts} l_a} \qquad (10b)$$

$$R_{bs} = \frac{w_{bs}}{\mu_0 h_{bs} l_a}, \qquad (10c)$$

where $\mu_{ys,i}$ and $\mu_{ts,i}$ are the yoke and tooth iron permeability, respectively, and $\mu_0 = 4\pi \times 10^{-7}$ (H/m) is the permeability of free space. Note that the prior two are dependent on the corresponding flux densities. The dependence $\mu(B)$ is obtained from the saturation characteristic of a commercial laminated steel and expressed as a piecewise linear function.

The unknown quantities in (7)-(10) are the fluxes $\Phi_{bs,i}$, $\Phi_{bs,i-1}$ and $\Phi_{bs,i+1}$. Values of $\Phi_{tsdq,i}$ and $\Phi_{ysdq,i}$ are obtained directly from the given air-gap flux density, according to assumption (i), and therefore represent input quantities. In order to obtain a square system with a unique solution, (7) needs to be formulated for each of the Q_{pp} slots under one pole pair, thereby constituting a system of Q_{pp} nonlinear algebraic equations. By noting that $\Phi_{bs,Q_{pp}+1} \equiv \Phi_{bs,1}$ and $\Phi_{bs,1-1} \equiv \Phi_{bs,Q_{pp}}$, the number of variables reduces to Q_{pp} as well and a square system of nonlinear algebraic equations is obtained. In the following section, the model of the analyzed 6PHIM will be synthesized and solved for different combinations of xy mmf and main flux density.

3.2 Calculation results

The calculations are performed using the data of the actual machine given in Table 3 in the Appendix. The main flux density distribution in the air-gap is given as:

$$B_{\delta dq}(\theta) = \hat{B}_\delta \cos\theta, \tag{11}$$

where $\hat{B}_\delta$ is the magnitude of the fundamental air-gap flux density and θ is the electrical angle, with $\theta = 0$ corresponding to the middle of the first tooth $(ts, 1)$ of the developed magnetic circuit model.

The mmf of each slot is calculated according to the currents of the top and bottom layer and the number of conductors per layer $(z_Q/2)$. An mmf distribution corresponding to the xy subspace is achieved by assigning appropriate currents to each phase according to [37]:

$$\begin{aligned} i_{a1,xy} &= \hat{I}_{xy} \cdot \cos\varphi_{xy} \\ i_{b1,xy} &= \hat{I}_{xy} \cdot \cos(\varphi_{xy} - 4\pi/3) \\ i_{c1,xy} &= \hat{I}_{xy} \cdot \cos(\varphi_{xy} - 2\pi/3) \\ i_{a2,xy} &= \hat{I}_{xy} \cdot \cos(\varphi_{xy} - 5\pi/6) \\ i_{b2,xy} &= \hat{I}_{xy} \cdot \cos(\varphi_{xy} - \pi/6) \\ i_{c2,xy} &= \hat{I}_{xy} \cdot \cos(\varphi_{xy} - 3\pi/2) \end{aligned} \tag{12}$$

The current magnitude $\hat{I}_{xy}$ will be held constant, whereas the phase angle φ_{xy} will be varied in order to change the position of the xy mmf. This angle will be referred to as the "xy phase shift", but it should be kept in mind that it is not actually current phase angle, but rather an artificial angle which reflects the displacement of the xy mmf with respect to the dq flux density. Introduction of this quantity allows for the analysis to be performed with different angular displacements between the fundamental and xy field, which is necessary as the latter is comprised dominantly of the 5^{th} and 7^{th} spatial harmonics. High-order space harmonics travel at lower speeds compared to the fundamental, and their mutual displacement will therefore change over time. The fundamental flux density and the 5^{th} harmonic of the xy mmf are displayed (conveniently scaled) in Fig. 2 for several values of φ_{xy}. The 5^{th} space harmonic alone is displayed to illustrate the physical meaning of the phase shift. However, it should be emphasized that, since each coil side of the winding is modeled individually, all space harmonics corresponding to the given winding layout are present and their influence is accounted for by the proposed magnetic circuit model. The stator winding distribution under one pole pair is displayed in Fig. 2, below the mmf waveforms.

The magnetic circuit model is solved for:

$$\begin{aligned} \hat{B}_\delta &\in \{0.4, 0.6, 0.9, 1.2\}\ \mathrm{T} \\ \varphi_{xy} &\in \left[0 : 30^\circ : 330^\circ\right] \\ \hat{I}_{xy} &= 5\ \mathrm{A} = \mathrm{const} \end{aligned} \tag{13}$$

Very low values of air-gap flux density can occur at large speeds, i.e. in the flux weakening region. The value of 1.2 T is not expected to ever occur and is chosen for purely theoretical reasons. After solving the model equations, yoke and tooth flux densities can be obtained according to (8), and the respective reluctances according to (10a) and (10b), respectively. Computed flux density distributions and corresponding reluctances obtained for $\hat{B}_\delta = 0.9$ T and $\varphi_{xy} = 90^\circ$, are shown in Fig. 3. It can be noticed that the addition of the xy current component leads to an increase of flux densities and reluctances in certain parts of the magnetic circuit and its decrease in other parts. Note that the influence of the xy current component on the reluctance is the most pronounced in those parts of the magnetic circuit that are already saturated by the main (dq) flux component.

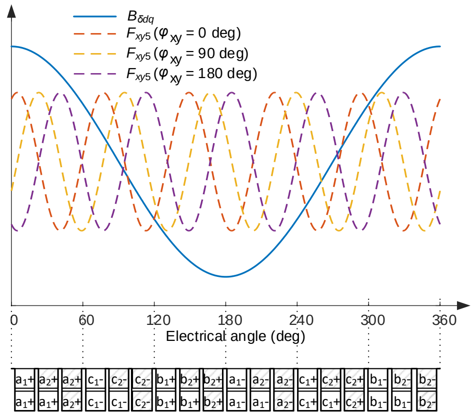

Fig. 2: Main flux density and xy mmf fifth harmonic distributions under one pole pair for different phase shifts

In order to quantify the saturation of the main flux path, the magnetic voltage across the stator yoke is calculated as:

$$U_{ysdq} = \int_0^\pi H_{ysdq}(\theta) r_{ys} d\theta \approx \frac{1}{2} \sum_{i=1}^{Q_{pp}} R_{ys,i} \left|\Phi_{ysdq,i}\right|, \tag{14}$$

where H_{ysdq} is the dq yoke field intensity attributed to the main flux and r_{ys} is the radius of the yoke centerline. Note that only the dq flux component is used in the calculation, but the influence of the xy current (mmf) component is included in calculation of the yoke reluctance, according to (10a). The magnetic voltage values are obtained for all the combinations given by (13). In order to quantify the influence of the xy currents on the main flux saturation, the ratio of stator yoke magnetic voltage values with and without the xy current component ("relative magnetic voltage") is calculated for each value the of main flux density and phase shift as:

$$u_{ys}^{(j,k)} = \frac{U_{ysdq}(\hat{B}_\delta^{(j)}, \varphi_{xy}^{(k)}, \hat{I}_{xy} = 5\ \mathrm{A})}{U_{ysdq}(\hat{B}_\delta^{(j)}, \hat{I}_{xy} = 0\ \mathrm{A})}, \tag{15}$$

where j and k denote the elements of corresponding arrays defined in (13). The relative magnetic voltage values are displayed in Fig. 4. The following conclusions can be derived from the given diagrams:

- The xy current component has a substantial effect on yoke saturation only when the main flux density is sufficiently high, in the sense that the magnetic circuit is previously saturated by the dq flux component;
- The magnetic voltage can either increase or decrease due to the xy current component, depending on the xy phase shift.

The results given in Fig. 4 clearly indicate that the xy current component has an influence on the saturation of the main flux path. Note that this influence is the most pronounced when the magnetic

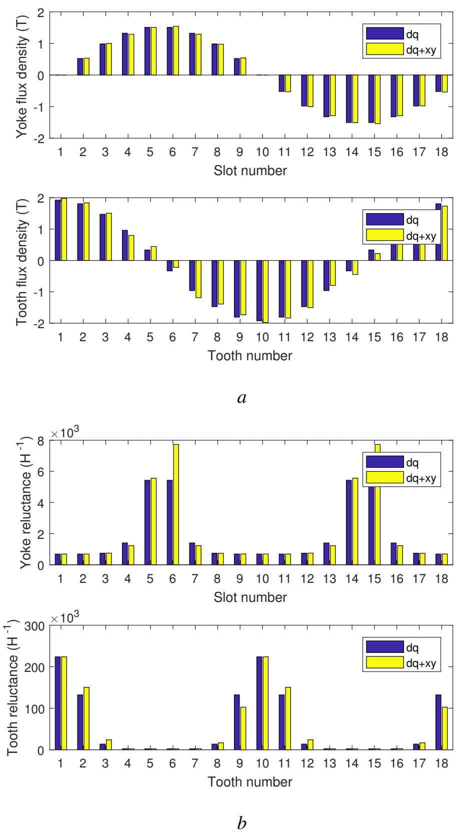

Fig. 3: Results obtained from the analytical model for $\hat{B}_\delta = 0.9$ T, $\varphi_{xy} = 90^\circ$
a Flux densities
b Reluctances

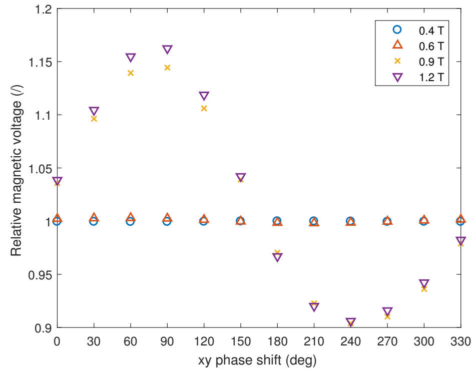

Fig. 4: Relative stator yoke magnetic voltage values as a function of the xy phase shift for different values of the main flux density (analytical model)

circuit is already saturated due to the dq flux component and for phase shifts around 90°. The results displayed in Fig. 3 were chosen to illustrate such conditions. Recall that the phase shift represents the position of the xy mmf component with respect to the main flux density. This phase shift is time dependent, therefore, the diagrams displayed in Fig. 4 correspond to time waveforms of the relative magnetic voltage. An increase of magnetic voltage means a larger magnetizing mmf (current) requirement for the same value of flux density, which consequently means a lower value of magnetizing inductance L_m. The opposite holds when the magnetic voltage is reduced. Seeing as the dq and xy fields travel at different angular velocities, the magnetizing inductance is expected to vary periodically. Note that these results are contrary to the previously adopted hypothesis (6), which indicates the presence of interplane cross-saturation. However, in order to obtain definite conclusions regarding the validity of the initial hypothesis, additional FEA and experimental verification are needed and will be presented in the following sections.

4 Finite element analysis

The FEA model of the analyzed machine is formed based on the electromagnetic design data given in Table 3. Rotor slot and yoke dimensions could not be measured precisely, so they are assumed based on common slot shapes and expected yoke flux density. The applied FEA software takes winding currents as inputs. Therefore, as constant air-gap flux density cannot be imposed, the concept will be somewhat different compared to the analytical procedure. Initially, the amplitudes of phase currents in the dq subspace that create the air-gap flux densities given by (13) are determined by running the model iteratively for each value. After this, the magnetics problem is solved for the following scenarios:

1) The winding currents are set to the values determined in the initial step (dq);
2) The winding currents are set to the values defined by (12) (xy). The analysis is conducted for all values of the phase angle φ_{xy} defined by (13). Note that φ_{xy} is modified according to the fundamental supply frequency;
3) The winding currents are set to the sum of the values corresponding to scenarios 1 and 2 ($dq + xy$).

The yoke field intensity distribution is obtained in each case. The diagrams for the unsaturated and saturated cases are displayed in Fig. 5. Note that, under saturated conditions ($\hat{B}_\delta = 0.9$ T), the field intensity obtained when the dq and xy current components act together differs significantly from the value obtained when only the dq current component is present, which indicates the presence of interplane cross-saturation. When the magnetic circuit is unsaturated ($\hat{B}_\delta = 0.4$ T), the influence of the xy current component is practically negligible. This confirms the conclusions of the analysis in section 3, as the influence of the xy component on the field distribution in the stator yoke is obviously much more pronounced when the magnetic circuit is saturated by the main flux.

In order to determine the influence of the xy current components on main flux path saturation, the yoke magnetic voltages in scenarios 1 and 3 need to be compared. Only the yoke magnetic voltage caused by the main flux is of interest. Therefore, the fundamental spatial component of the yoke flux density is obtained for each scenario, and the magnetic voltage is determined as:

$$U_{ysdq} = \int_0^\pi \frac{B_{ys1}(\theta)}{\mu(\theta)} r_{ys} d\theta, \tag{16}$$

where B_{ys1} denotes the fundamental spatial component of the yoke flux density. The magnetic material permeability is calculated as:

$$\mu(\theta) = \frac{B_{ys}(\theta)}{H_{ys}(\theta)}, \tag{17}$$

where B_{ys} and H_{ys} are the total flux density and field intensity at the point (r_{ys}, θ) on the stator yoke centerline. The relative stator yoke magnetic voltage values are calculated by dividing the values obtained from (16) in scenarios 1 and 3 and given in Fig. 6. These results are very similar to those obtained from the analytical magnetic circuit model (Fig. 4). Of course, an exact match cannot be expected, as the air-gap flux density in the FEA model changes with the addition of the xy current component, and the magnetic circuit model itself is of limited accuracy. For instance, the leakage flux generated by dq currents was neglected in the magnetic circuit model. However, this flux is very pronounced in the FEA model at 1.2 T, as the magnetic circuit is highly saturated at such a high air-gap flux density, hence the required dq current is several times larger than the rated value. Nevertheless, the FEA confirms the conclusions derived in section 3. The influence of the xy component is significant if the magnetic circuit is already saturated due to the main flux. The level of saturation, i.e. the magnetic voltage, can decrease or increase depending on the position of the xy mmf wave (phase shift φ_{xy}). The results obtained from FEA confirm the presence of interplane cross-saturation indicated by the results of the analytical model.

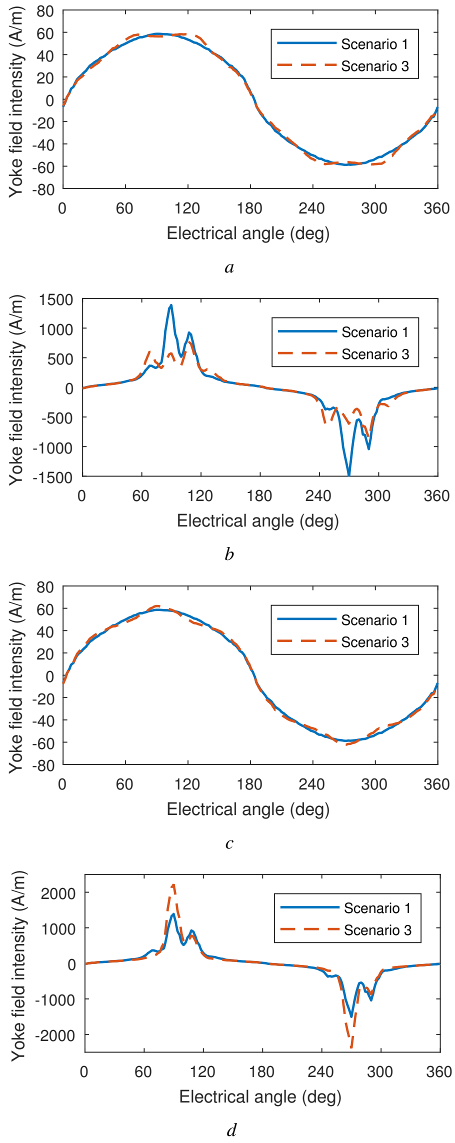

Fig. 5: Stator yoke field intensity obtained using FEA
a $\hat{B}_\delta = 0.4$ T, $\varphi_{xy} = 270°$
b $\hat{B}_\delta = 0.9$ T, $\varphi_{xy} = 270°$
c $\hat{B}_\delta = 0.4$ T, $\varphi_{xy} = 90°$
d $\hat{B}_\delta = 0.9$ T, $\varphi_{xy} = 90°$

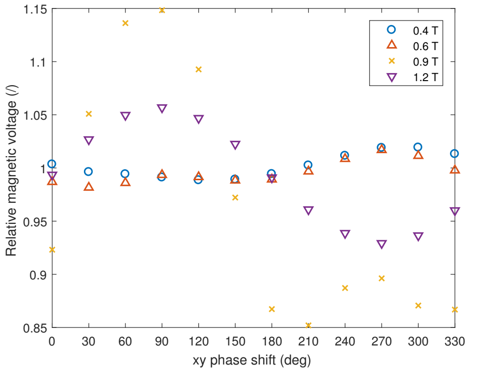

Fig. 6: Relative stator yoke magnetic voltage as a function of the xy phase shift for different values of the main flux density (FEA)

5 Experimental verification

The influence of xy current components on the main flux saturation will be studied by observing the currents of the 6PHIM. For this purpose, measurements are performed in three operating modes characterized by the applied voltage components:

1) dq voltage supply,
2) xy voltage supply, and
3) $dq + xy$ voltage supply.

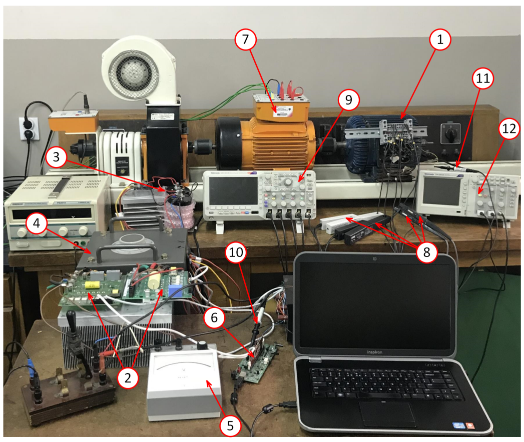

Fig. 7: Experimental setup: 1–6PHIM, 2–three-phase inverter boards, 3–DC bus, 4–variac, 5–DC bus voltage measurement, 6–microcontroller, 7–auxiliary motor, 8–current probes, 9–four-channel oscilloscope, 10–voltage probe (PWM1 signal), 11–voltage probe (air-gap voltage), 12–two-channel oscilloscope

IET Research Journals, pp. 1–11

Table 1 Supply voltage information

DC bus voltage	Component (subspace)	Modulation index	Phase voltage fundamental
300 V	dq	0.84	89 Vrms
300 V	xy	0.16	17 Vrms
600 V	dq	0.92	196 Vrms
600 V	xy	0.08	17 Vrms

The tests are performed for different levels of saturation. The saturation level, i.e. the main flux density, is varied by changing the amplitude of the dq component of supply voltage.

The experimental setup is displayed in Fig. 7. The 6PHIM is supplied from two three-phase inverters connected to a common DC bus and controlled from a 32-bit digital signal controller with 6 PWM channels. According to [34], such a configuration is applicable when the neutral points of the two three-phase windings are separated. The DC voltage is obtained from a three-phase diode bridge rectifier supplied from a variable autotransformer. The PWM outputs are controlled in such a way that the initial phase angle corresponding to the first channel is always equal to zero, whereas the phase angles corresponding to other channels are assigned so that the required voltage components (dq or xy) are obtained. The four-channel oscilloscope is used for the measurement of four phase currents – two in one three-phase winding, and two in the other. As the neutral point of each three-phase winding is isolated, the remaining two currents are easily calculated. The two-channel oscilloscope is used for: a) measurement of the voltage signal on the first PWM channel (PWM1 further on), which is used for time-synchronization of the current waveforms obtained in different operating modes, and b) measurement of the induced voltage of a single-turn coil placed under one pole of the 6PHIM (approximately proportional to the air-gap flux). The auxiliary motor is a four-pole induction motor used for running the 6PHIM at approximately no-load speed in operating mode 2. In operating modes 1 and 3, the auxiliary motor is disconnected from the supply and the 6PHIM is operated in no-load conditions.

The tests are conducted for two values of DC bus voltage – $U_{dc} = 300$ V and $U_{dc} = 600$ V. Operation with $U_{dc} = 300$ V will be referred to as the "unsaturated case", whereas operation with $U_{dc} = 600$ V represents the "saturated case". The fundamental voltage component corresponds to the rated frequency of 50 Hz (see Table 3 in the Appendix). The fundamental of xy voltage is maintained equal at both DC voltage levels by setting the appropriate values of the modulation index, so that approximately equal xy currents are obtained in both cases. The values of the modulation indices and the corresponding rms values of the supply voltage fundamental for each component and DC voltage level are given in Table 1. The fundamental component of dq voltage was set to the same value in modes 1 and 3, in order to obtain an approximately equal air-gap flux densities in these two cases. Note that the sum of the modulation indices corresponding to the dq and xy component may not exceed 1, otherwise overmodulation would occur in operating mode 3 (pure sinusoidal PWM is used, without zero-sequence injection). Obviously, the phase voltage could have been decreased by reducing the modulation index without lowering the DC bus voltage. However, this would lead to a reduction of the fundamental harmonic of current, while the ripple would remain unchanged, thereby reducing the measurement accuracy. This is a significant matter, as the oscilloscopes provide only 8-bit vertical resolution.

The oscilloscope screenshots of phase current waveforms corresponding to all three operating modes are shown in Figs. 8 and 9. The output/input ratio of each probe was set to 10 mV/A. The motor was operated at no-load in modes 1 and 3, and rotated at approximately no-load speed by means of the auxiliary motor in operating mode 2. It was necessary to rotate the machine under xy supply in order to achieve the same rotor cage reaction to xy current components as in mode 3. Note that the currents in mode 1 are highly unbalanced, even though the supply voltages form a balanced six-phase system. This is the consequence of the winding asymmetry, i.e. the different winding distribution of the first and second three-phase winding (see Fig. 2). Therefore, an xy current component is present even under balanced supply. This does not represent a problem though, as the influence of the additional xy component corresponding to mode 2 can be observed regardless of the inherent xy components in mode 1. The displayed waveforms indicate that the currents corresponding to 300 Vdc are sinusoidal in all three operating modes with no notable distortion. On the other hand, the currents corresponding to 600 Vdc exhibit a certain amount of distortion, especially in operating mode 3.

In order to better visualize the influence of the xy currents on the saturation of the magnetic circuit, the following waveforms are overlapped in Fig. 10, representing:

- the sum of currents in operating modes 1 and 2, and
- the current in operating mode 3.

All waveforms were synchronized in time with respect to the fundamental harmonic of the measured PWM1 signal. The PWM1 signal was recorded on a separate two-channel oscilloscope. In order to obtain the current and PWM1 measurements at the same time instant, a single-shot external trigger was applied to both oscilloscopes.

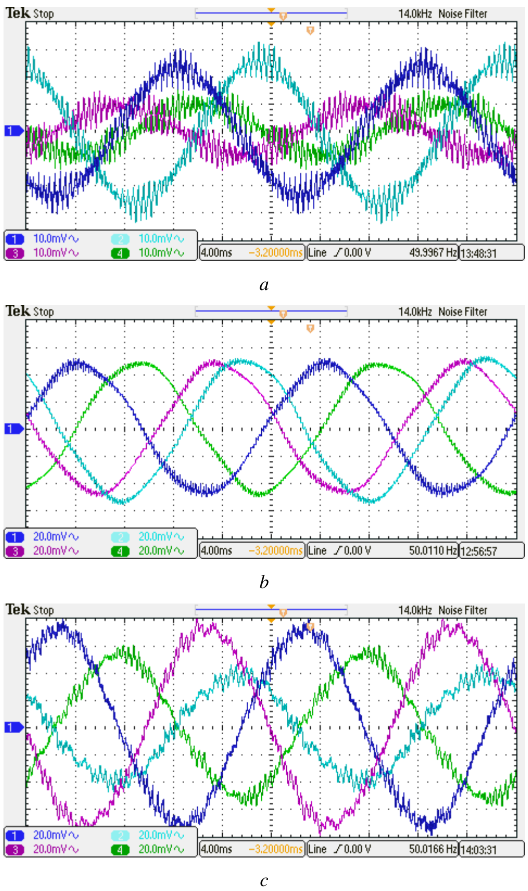

Fig. 8: Current waveforms, 300 Vdc supply
a Operating mode 1
b Operating mode 2
c Operating mode 3

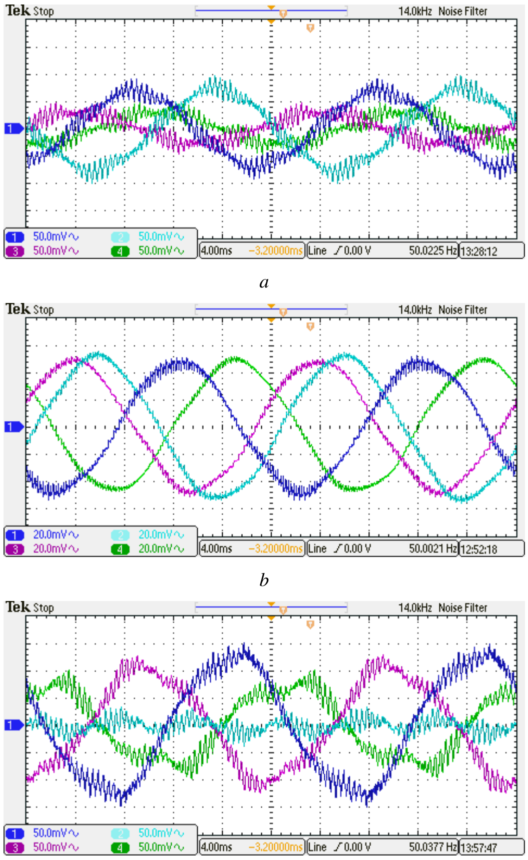

Fig. 9: Current waveforms, 600 Vdc supply
a Operating mode 1
b Operating mode 2
c Operating mode 3

If the decoupling assumption were correct, the waveforms obtained by superposition of currents in mode 1 and mode 2 should be nearly identical to those obtained in mode 3. According to Fig. 10*a*, this is true for waveforms obtained for the unsaturated case (300 Vdc). On the other hand, the waveforms obtained in the saturated case (600 Vdc) differ noticeably (Fig. 10*b*). This indicates that the dq and xy subspaces are not decoupled when the magnetic circuit is saturated, i.e. that interplane cross-saturation is present.

The second channel of the two-channel oscilloscope was used for measuring the emf induced in a test coil placed under one pole of the stator. This emf can be considered approximately proportional to the air-gap flux. However, a certain amount of tooth-tip and zig-zag leakage is inevitably present in the flux linkage of the test coil. For purely exemplary purposes, the recorded emf waveform corresponding to 600 Vdc, operating mode 1, is shown in Fig. 11. The magnitude of the fundamental of air-gap flux density is obtained as:

$$\hat{B}_\delta = \frac{pE_1}{\sqrt{2}\pi D_{si} l_a f_1}, \tag{18}$$

where E_1 is the rms value of the test coil emf fundamental. All other quantities from (18) are defined in Table 3 in the Appendix. The obtained values of fundamental air-gap flux density in operating modes 1 and 3, in both the unsaturated and saturated case, are given in Table 2. These values are very close to those selected in the analytical approach and FEA, see (13). It is important to note that the flux densities in mode 1 and 3 differ very slightly, which is most likely the consequence of increased leakage flux due to xy current components in mode 3. The air-gap flux density under rated operating conditions (rated load and 180 V per phase) was determined to be 0.78 T. By observing the results of Table 2 and considering that the magnetic circuit is moderately saturated under rated operating conditions, it follows that saturation is negligible at 300 Vdc, whereas it is highly pronounced at 600 Vdc.

The phase current waveforms are not sufficient to determine the influence of the xy current components on the saturation of the main flux path. Therefore, an additional analysis of dq current components is necessary. The time-varying amplitude of the space vector of the

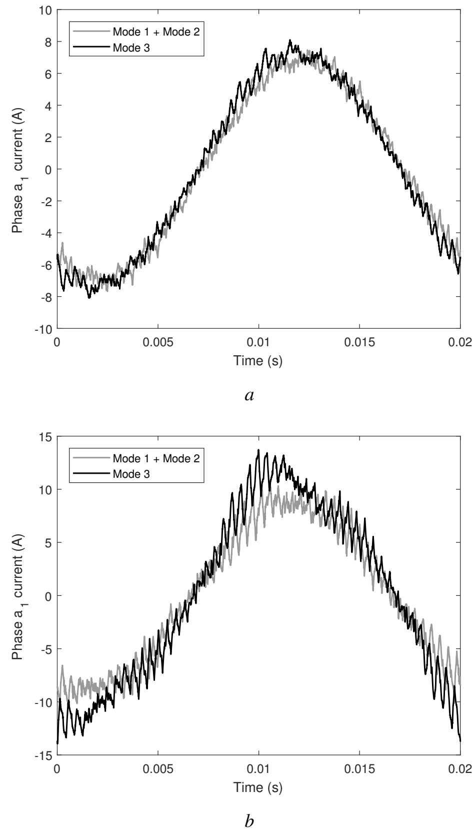

Fig. 10: Comparison of phase a_1 current waveforms in operating mode 3 and the sum of currents in operating modes 1 and 2
a Unsaturated case (300 Vdc)
b Saturated case (600 Vdc)

Table 2 Test coil fundamental emf and air-gap flux density values

DC bus voltage (operating mode)	Emf fundamental	Air-gap flux density
300 V (1)	0.658 V	0.41 T
300 V (3)	0.672 V	0.42 T
600 V (1)	1.453 V	0.90 T
600 V (3)	1.479 V	0.92 T

dq component is calculated as:

$$\hat{i}_{dq} = |i_{ds} + \mathrm{j}i_{qs}| \tag{19}$$

Note that this value corresponds to the magnetizing current defined by (6) if the rotor currents are equal to zero. This is approximately true under no-load conditions. Therefore, it will be considered that $\hat{i}_{dq} \approx i_m$, and the dq current vector amplitude will be referred to as the magnetizing current further on. The magnetizing current waveforms corresponding to the sum of currents of modes 1 and 2 and the currents of mode 3 are compared. The phase current spectral components above 1 kHz were previously removed in order to reduce the ripple and allow better visualization. The obtained values for the unsaturated and saturated cases are shown in Fig. 12. All waveforms indicate a presence of a backward component (100 Hz), which can be attributed to many different factors, such as winding asymmetry, rotor eccentricity, etc. The waveforms under unsaturated conditions (Fig. 12*a*) are very similar, indicating that no interplane cross-saturation has taken place. However, the waveforms under saturated conditions (Fig. 12*b*) differ significantly. Two major differences can be observed:

- the average value of the magnetizing current, which corresponds to the forward component, is greater in mode 3 than in mode 1+2 by approximately 10%, and
- the variations of the magnetizing current are greater in mode 3.

Both phenomena can be attributed to interplane cross-saturation. The increase of the average of the magnetizing current indicates a greater average reluctance of the main flux path over one period of the fundamental frequency. Recall that the magnetic voltage, which is proportional to the yoke reluctance, varies periodically over time, see Figs. 4 and 6. The more pronounced oscillations of the magnetizing current can be attributed to the periodical variations of the reluctance due to the xy component. This can be observed from Figs. 4 and 6.

The influence of interplane cross-saturation is present in the xy plane as well. This can be observed from Fig. 13, where the waveforms of current i_x in the saturated and unsaturated cases are displayed. A comparison is made between the current corresponding to operating mode 3 and the sum of currents corresponding to modes 1 and 2. In the unsaturated case (Fig. 13*a*), the two waveforms are nearly identical. In the saturated case (Fig. 13*b*) there is a significant increase in the current magnitude. The Fourier analysis of the waveforms reveals that the fundamental (50 Hz) component is the most affected, with a relative increase of nearly 40%. Higher order harmonics are also inflicted by saturation, but are still much lower than the fundamental.

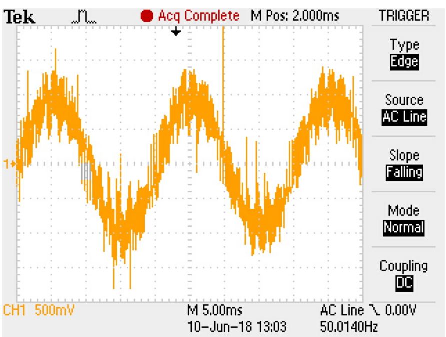

Fig. 11: Test coil induced emf waveform (operating mode 1, 600 Vdc)

6 Discussion

Results obtained from the magnetic circuit model, FE analysis and experiment confirm the presence of mutual coupling between the dq and xy subspaces under saturated conditions. This implies a requirement for an improved multiphase machine model which includes this phenomenon, termed interplane cross-saturation. A summary of the obtained results is in order:

1) The dq and xy subspaces are decoupled under unsaturated conditions (see Figs. 12*a* and 13*a*);
2) The addition of xy current components under saturated conditions increases the magnetizing (dq) current component (see Fig. 12*b*);
3) Saturation of the magnetic circuit, i.e. the increase of magnetizing (dq) current increases the xy current component (see Fig. 13*b*);
4) The xy current component does not affect the air-gap flux density, regardless of the saturation level (see Table 2).

These observations can be used as a starting point to formulate a model that can adequately deal with the observed saturation effects. The intention is to retain the basic model formulation similar to (1)-(6) and to accommodate the findings of this paper through modifications of the flux linkage equations (3). Since any such new

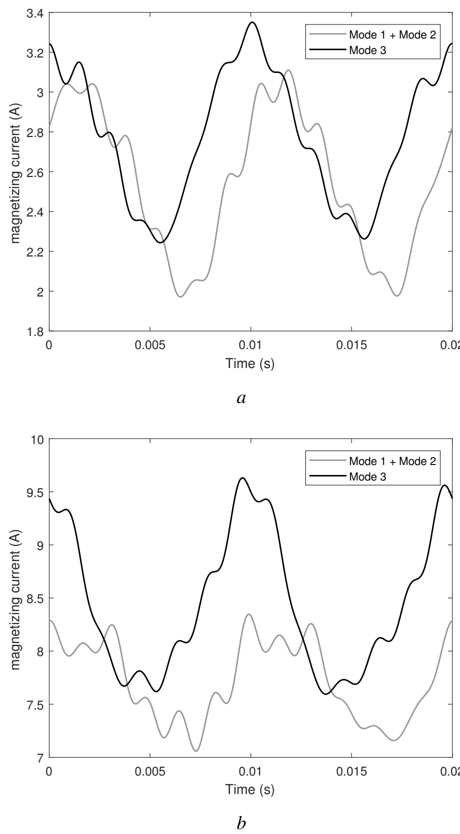

Fig. 12: Comparison of magnetizing current waveforms in operating mode 3 and the sum of currents in modes 1 and 2
a Unsaturated case (300 Vdc)
b Saturated case (600 Vdc)

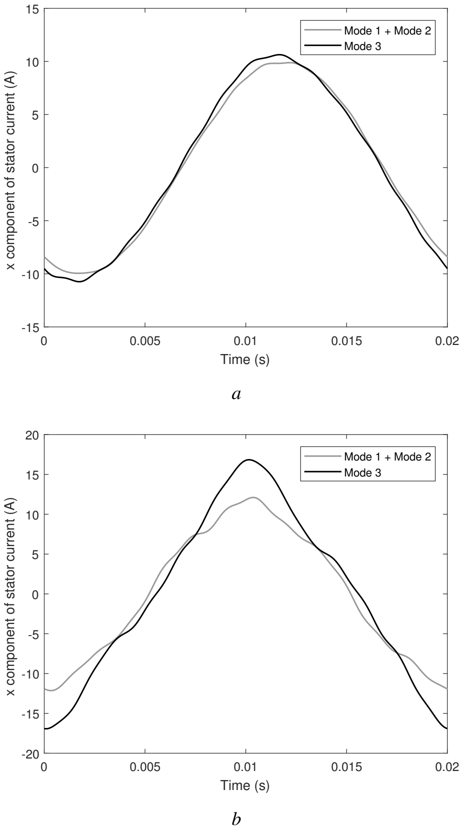

Fig. 13: Comparison of x current component waveforms in operating mode 3 and the sum of currents in modes 1 and 2
a Unsaturated case (300 Vdc)
b Saturated case (600 Vdc)

model would inevitably require parameter identification and subsequent experimental verification, its exact formulation is postponed until these conditions are met.

7 Conclusion

Interplane cross-saturation, i.e. mutual coupling between the orthogonal subspaces in a VSD model of a saturated multiphase machine, was investigated. The fundamental frequency xy components characteristic for post-fault and power-sharing operating modes were considered. The analysis was carried out for an asymmetrical six-phase induction machine. The research was conducted through analytical considerations, finite element analysis and experimentally. Analytical and FEA results have demonstrated that the reluctances of ferromagnetic parts of the machine depend on the xy current components and the observed time instant, i.e. the displacement between the main flux density and xy mmf component. Experimental results have demonstrated that the dq current component is affected by superposition of xy supply voltage component to the preexisting dq component. However, this effect is significant only if the machine is saturated prior to the superposition of the xy component. Therefore, the initial assumption, stating that the VSD model can be expanded by simply including a variable magnetizing inductance dependent on the dq current components into the existing unsaturated model, was shown to be incorrect. The results of all analyses indicate that interplane cross-saturation is present and needs to be taken into account for control and modeling purposes. The results obtained in this paper reveal a need to develop a new multiphase machine model or modify the existing models in order to include interplane cross-saturation. Guidelines for obtaining such a model were given in this paper. The exact formulation and verification of the model will be the focus of future research.

8 References

1 Levi, E., Bojoi, R., Profumo, F., *et al.*: 'Multiphase induction motor drives - a technology status review', *IET Electric Power Applications*, 2007, **1**, (4), pp. 489–516

2 Levi, E.: 'Multiphase electric machines for variable-speed applications', *IEEE Transactions on Industrial Electronics*, 2008, **55**, (5), pp. 1893–1909

3 Levi, E., Barrero, F., Duran, M.J.: 'Multiphase machines and drives-revisited', *IEEE Transactions on Industrial Electronics*, 2016, **63**, (1), pp. 429–432

4 Levi, E., Jones, M., Vukosavic, S., *et al.*: 'A novel concept of a multiphase, multimotor vector controlled drive system supplied from a single voltage source inverter', *IEEE Transactions on Power Electronics*, 2004, **19**, (2), pp. 320–335

5 Hofmann, H., Sanders, S.R., Sullivan, C.R.: 'Stator-flux-based vector control of induction machines in magnetic saturation', *IEEE Transactions on Industry Applications*, 1997, **33**, (4), pp. 935–942

6 Slemon, G.R.: 'Equivalent circuits for transformers and machines including nonlinear effects', *IEE Proceedings*, 1953, **100**, pp. 129–143

7 Brown, J.E., Kovacs, K.P., Vas, P.: 'A method of including the effects of main flux path saturation in the generalized equations of a.c. machines', *IEEE Transactions on Power Apparatus and Systems*, 1983, **PAS-102**, (1), pp. 96–103

8 Hallenius, K.E., Vas, P., Brown, J.E.: 'The analysis of a saturated self-excited asynchronous generator', *IEEE Transactions on Energy Conversion*, 1991, **6**, (2), pp. 336–345

9 Levi, E.: 'Applications of the current state space model in analyses of saturated induction machines', *Electric Power Systems Research*, 1994, **31**, (3), pp. 203–216

10 Levi, E., Krzeminski, Z.: 'Main flux-saturation modelling in d-q axis models of induction machines using mixed current-flux state-space models', *European Transactions on Electrical Power*, 1996, **6**, (3), pp. 207–215

11 Levi, E., Levi, V.A.: 'Impact of dynamic cross-saturation on accuracy of saturated synchronous machine models', *IEEE Transactions on Energy Conversion*, 2000, **15**, (2), pp. 224–230

12 Therrien, F., Wang, L., Jatskevich, J., *et al.*: 'Efficient explicit representation of ac machines main flux saturation in state-variable-based transient simulation packages', *IEEE Transactions on Energy Conversion*, 2013, **28**, (2), pp. 380–393

13 Wang, L., Jatskevich, J., Pekarek, S.D.: 'Modeling of induction machines using a voltage-behind-reactance formulation', *IEEE Transactions on Energy Conversion*, 2008, **23**, (2), pp. 382–392

14 Wang, L., Jatskevich, J.: 'Including magnetic saturation in voltage-behind-reactance induction machine model for emtp-type solution', *IEEE Transactions on Power Systems*, 2010, **25**, (2), pp. 975–987

15 Therrien, F., Chapariha, M., Jatskevich, J.: 'Constant-parameter voltage-behind-reactance induction machine model including main flux saturation', *IEEE Transactions on Energy Conversion*, 2015, **30**, (1), pp. 90–102

16 Yepes, A.G., Riveros, J.A., Doval.Gandoy, J., *et al.*: 'Parameter identification of multiphase induction machines with distributed windings part 1: Sinusoidal excitation methods', *IEEE Transactions on Energy Conversion*, 2012, **27**, (4), pp. 1056–1066

17 Che, H.S., Abdel-Khalik, A.S., Dordevic, O., *et al.*: 'Parameter estimation of asymmetrical six-phase induction machines using modified standard tests', *IEEE Transactions on Industrial Electronics*, 2017, **64**, (8), pp. 6075–6085

18 Nelson, R.H., Krause, P.C.: 'Induction machine analysis for arbitrary displacement between multiple winding sets', *IEEE Transactions on Power Apparatus and Systems*, 1974, **PAS-93**, (3), pp. 841–848

19 Lipo, T.A. 'A d-q model for six phase induction machines'. International Conf. Electrical Machines, Athens, Greece, 1980,

20 Singh, G.K.: 'Modeling and experimental analysis of a self-excited six-phase induction generator for stand-alone renewable energy generation', *Renewable Energy*, 2008, **33**, (7), pp. 1605–1621

21 Abdel-Khalik, A.S., Ahmed, S., Elserougi, A.A., *et al.*: 'A voltage-behind-reactance model of five-phase induction machines considering the effect of magnetic saturation', *IEEE Transactions on Energy Conversion*, 2013, **28**, (3), pp. 576–592

22 Amiri, N., Ebrahimi, S., Chapariha, M., *et al.*: 'Voltage-behind-reactance model of six-phase synchronous machines considering stator mutual leakage inductance and main flux saturation', *Electric Power Systems Research*, 2016, **138**, pp. 155–164

23 Pereira, L.A., Scharlau, C.C., Pereira, L.F.A., *et al.*: 'Influence of saturation on the airgap induction waveform of five-phase induction machines', *IEEE Transactions on Energy Conversion*, 2012, **27**, (1), pp. 29–41

24 Duran, M.J., Prieto, I.G., Bermudez, M., *et al.*: 'Optimal fault-tolerant control of six-phase induction motor drives with parallel converters', *IEEE Transactions on Industrial Electronics*, 2016, **63**, (1), pp. 629–640

25 Rubino, S., Bojoi, R., Cavagnino, A., *et al.* 'Asymmetrical twelve-phase induction starter/generator for more electric engine in aircraft'. 2016 IEEE Energy Conversion Congress and Exposition (ECCE), 2016, pp. 1–8

26 Tani, A., Serra, G., Mengoni, M., *et al.* 'Dynamic stator current sharing in quadruple three-phase induction motor drives'. IECON 2013 - 39th Annual Conference of the IEEE Industrial Electronics Society, 2013, pp. 5173–5178

27 Mengoni, M., Sala, G., Zarri, L., *et al.* 'Control of a fault-tolerant quadruple three-phase induction machine for more electric aircrafts'. IECON 2016 - 42nd Annual Conference of the IEEE Industrial Electronics Society, 2016, pp. 5747–5753
28 Zoric, I., Jones, M., Levi, E.: 'Arbitrary power sharing among three-phase winding sets of multiphase machines', *IEEE Transactions on Industrial Electronics*, 2018, **65**, (2), pp. 1128–1139
29 Luise, F., Pieri, S., Mezzarobba, M., *et al.*: 'Regenerative testing of a concentrated-winding permanent-magnet synchronous machine for offshore wind generation - part i: Test concept and analysis', *IEEE Transactions on Industry Applications*, 2012, **48**, (6), pp. 1779–1790
30 Zabaleta, M., Levi, E., Jones, M.: 'A novel synthetic loading method for multiple three-phase winding electric machines', *IEEE Transactions on Energy Conversion*, 2018, pp. 1–9
31 Slemon, G.R.: 'Modelling of induction machines for electric drives', *IEEE Transactions on Industry Applications*, 1989, **25**, (6), pp. 1126–1131
32 Vassent, E., Meunier, G., Sabonnadiere, J.C.: 'Simulation of induction machine operation using complex magnetodynamic finite elements', *IEEE Transactions on Magnetics*, 1989, **25**, (4), pp. 3064–3066
33 Marti, J.R., Louie, K.W.: 'A phase-domain synchronous generator model including saturation effects', *IEEE Transactions on Power Systems*, 1997, **12**, (1), pp. 222–229
34 Bojoi, I.R. 'Analysis, design and implementation of a dual three-phase vector controlled induction motor drive'. PhD thesis. Politecnico di Torino. Turin, Italy, 2002
35 Zhao, Y., Lipo, T.A.: 'Space vector pwm control of dual three-phase induction machine using vector space decomposition', *IEEE Transactions on Industry Applications*, 1995, **31**, (5), pp. 1100–1109
36 Zoric, I., Jones, M., Levi, E. 'Vector space decomposition algorithm for asymmetrical multiphase machines'. 19th International Symposium on Power Electronics, Ee 2017, 2017, pp. 1–6
37 Levi, E. 'Multiphase ac machines'. Irwin, J.D., editor. The Industrial Electronics Handbook on Power Electronics and Motor Drives. (CRC Press, 2011. pp. 1–31)
38 Hadiouche, D., Razik, H., Rezzoug, A.: 'On the modeling and design of dual-stator windings to minimize circulating harmonic currents for vsi fed ac machines', *IEEE Transactions on Industry Applications*, 2004, **40**, (2), pp. 506–515
39 Vas, P., Brown, J.E., Hallenius, K.E.: 'Cross-saturation in smooth-air-gap electrical machines', *IEEE Transactions on Energy Conversion*, 1986, **EC-1**, (1), pp. 103–112
40 Lipo, T.A.: 'Introduction to AC Machine Design'. (John Wiley & Sons, Inc., 2017)

9 Appendix

The rated data and dimensions of the analyzed 6PHIM are given in Table 3. The 6PHIM was obtained by rewinding an existing three-phase machine. Due to a limited number of stator slots and the requirement to keep the same number of poles in order to avoid excessive yoke saturation, the winding was executed with 1.5 slots per pole and phase. The given rated power corresponds to that of the original three-phase machine, which is a reasonable assumption considering that the cross-section of the conductors was retained. A thermal test would need to be conducted in order to determine the rated power of the 6PHIM.

Table 3 Machine data

Parameter	Designation (Unit)	Value
Rated power (estimated)	P_n (W)	4000
Rated frequency	f_1 (Hz)	50
Rated current	I_n (A)	5.2
Rated voltage (per phase)	U_{nf} (V)	180
No. of poles	$2p$ (/)	4
No. of stator slots	Q_s (/)	36
No. of rotor slots	Q_r (/)	28
No. of turns/phase	N_s (/)	264
No. of conductors/slot	z_Q (/)	44
Conductor diameter	d (mm)	1.0
Outer stator diameter	D_{se} (mm)	184
Inner stator diameter	D_{si} (mm)	116
Air gap length	δ (mm)	0.5
Stack length	l_a (mm)	125
Stator slot height	h_{ss} (mm)	16
Stator slot width	w_{ss} (mm)	6.2
Stator slot opening height	h_{bs} (mm)	1.2
Stator slot opening width	w_{bs} (mm)	1.8
Stator tooth width	w_{ts} (mm)	5.4
Stator yoke height	h_{ys} (mm)	17